

# Global Structure of Buffeting Flow on Transonic Airfoils

J.D. Crouch, A. Garbaruk, D. Magidov, and L. Jacquin

**Abstract** The flow field associated with transonic airfoil buffet is investigated using a combination of global-stability theory and experimental data. The theory is based on perturbing a steady flow field obtained from the Reynolds-averaged Navier–Stokes equations. Linearized perturbations are described by an eigenvalue problem, with the frequency and growth rate given by the eigenvalue and global-flow structure provided by the eigenfunction. The experiments provide both steady and unsteady information on the airfoil surface and in the flow downstream of the shock. The theory and experiment show good agreement for the buffet onset conditions – including the critical angle of attack and the buffet-onset frequency. The post-buffet flow structure is also in good agreement, and shows a shock oscillation phase locked to an oscillating shear layer downstream of the shock.

**Keywords** Buffet · Global instability · Transonic flow · RANS · Unsteady flow

## 1 Introduction

The upper surface flow over transonic airfoils is characterized by a supersonic zone followed by a shockwave and a subsonic pressure recovery. As the airfoil lift is increased with angle of attack, the shock becomes stronger. At some angle of attack, the flow separates – either from the trailing edge, or locally as a bubble at the foot of the shock. Further increase in the angle of attack results in an onset

---

J.D. Crouch (✉)  
Boeing Commercial Airplanes, Seattle, USA  
e-mail: jeffrey.d.crouch@boeing.com

A. Garbaruk and D. Magidov  
Saint-Petersburg Polytechnic University, St. Petersburg, Russia  
e-mail: agarbaruk@mail.ru, dmagidov@rscac.spb.ru

L. Jacquin  
ONERA-Fundamental/Experimental Aerodynamics Dept, Meudon, France  
e-mail: laurent.jacquin@onera.fr

of large-scale unsteadiness, leading to large oscillations in the sectional lift. This unsteadiness has been shown to result from global flow instability [1]. The unsteadiness is characterized by phased-locked oscillations of the shock and the separated shear layer. Results from the global-instability analysis are in good agreement with earlier experiments on a NACA 0012 airfoil [2]. However, these earlier experiments do not provide details about the flow structure or spectral information at the onset conditions.

More recent experiments on a modern supercritical airfoil have captured the details of the buffeting flow field in the neighbourhood of the buffet onset [3]. Subsequent results from unsteady Reynolds-averaged Navier–Stokes (URANS) equations show good agreement with the experiments [4, 5]. The URANS results show a dependence on the turbulence model used, as well as a potential influence from the tunnel walls.

Here we combine the global-instability theory [1] and the detailed experiments [3] to provide a description of the origins and flow structure of airfoil buffeting.

## 2 Problem Formulation

### 2.1 Global Stability Analysis

Theoretical predictions are based on a global stability analysis of a steady-state solution obtained from the Reynolds-averaged Navier–Stokes (RANS) equations – see [1] for expanded details. The compressible form of the S-A turbulence model is used [6], including the compressibility correction [7]. The total flow is described by the state vector  $q = \{\rho, u, v, T, \tilde{\nu}\}$ , where  $\rho$  is the density,  $u, v$  are the velocities in the  $x$ -,  $y$ -directions,  $T$  is the temperature, and  $\tilde{\nu}$  is a scaled form of the eddy viscosity.

The total flow solution is split into a steady-state solution  $\bar{q}(x, y)$  and an unsteady perturbation  $q'(x, y, t)$ ,  $q = \bar{q} + q'$ . Substituting this into the RANS equations, removing terms governing  $\bar{q}$ , and linearizing with respect to  $q'$  provides a set of equations governing  $q'$ . The unsteady perturbation is then expanded in modal form,  $q'(x, y, t) = \hat{q}(x, y) \exp(-i\omega t)$ . This leads to an eigenvalue problem governing the complex frequency  $\omega$  and the unsteady-disturbance mode shape  $\hat{q}$ .

The governing equations are discretized using a finite-different approximation. The steady flow is obtained using the NTS code [8]. The perturbation equations are then solved on the same grid using a hybrid scheme, which blends a fourth-order centered scheme with a third-order upwind scheme [1]. The size of the final eigenvalue problem is  $O(10^6)$ . This is solved using the implicitly restarted Arnoldi method [9]. Using the shift-invert mode, a small number of eigenvalues can be calculated in the neighborhood of a prescribed frequency.

In the limit of an incompressible laminar basic flow, the analysis simplifies to the approach used by Jackson [10] and Zebib [11] for the analysis of vortex shedding behind cylinders. Results from the current approach for the onset of vortex shedding behind cylinders are shown to be in very good agreement with experiments [1].

For high-Reynolds-number transonic flows, a turbulence model is required to obtain the basic-state flow. In addition, shock smoothing is used to prevent “ringing” in the eigenmode response. The shock smoothing (in conjunction with the local grid spacing) affects the shock thickness; coarser grids and increased smoothing yield a thicker shock, which enhances stability of the steady base flow. Physically, the thicker shock is representative of the time-averaged flow observed once shock buffeting has occurred. Small levels of smoothing on a fine grid do not substantially alter the results.

## 2.2 Experimental Setup and Signal Processing

The experiment considered here is that conducted by Jacquin et al. [3] in the continuous closed-circuit transonic wind tunnel S3Ch of the Fundamental and Experimental Aerodynamics Department of ONERA. The model was a supercritical airfoil OAT15A characterized by a 12.3% thickness-to-chord ratio, a 230 mm chord length and a 780 mm span (aspect ratio  $AR \approx 3.4$ ). Average Reynolds number was  $Re_c = 3(10)^6$  based on the chord length. Laminar-turbulent transition was fixed on the model using a Carborundum strip located at  $x/c = 7\%$  from the leading edge. The Mach number  $M$  was varied between 0.70 and 0.75 and the flow incidence  $\alpha$ , controlled by means of adaptable walls, between  $2.5^\circ$  to  $3.91^\circ$ . The measurements comprised surface flow visualisations by oil and sublimating products, steady and unsteady pressure by 68 static pressure taps and 36 unsteady Kulite<sup>TM</sup> pressure transducers (in the central section of the wing), flow field characterizations by Shlieren films, and velocity fields by means of a two component laser-Doppler velocimeter. At  $M = 0.73$ , the value considered herein, unsteady pressure signals revealed perturbation onset at  $\alpha = 3.1^\circ$ , and perfectly periodic signals indicating buffet were obtained for incidences comprised between  $\alpha = 3.25^\circ$  and  $3.9^\circ$ .

The value  $\alpha = 3.5^\circ$  was selected for a full characterisation of the unsteady velocity field with the laser-Doppler velocimeter. As shown in Fig. 1, the meshing used consisted in a series of vertical lines located in the airfoil symmetry plane with variable meshes with separations varying from 2 to 0.5 mm. The phase-averaged technique introduced by Hussain and Reynolds [12] has been applied to this data, following the method described in Forestier et al. [13]. The technique can separate the ‘coherent’ motion, related to the periodic excitation, from the random fluctuating part. A component of the velocity,  $u(\underline{x}, t)$  for instance, is decomposed into three contributions,  $u(\underline{x}, t) = \bar{u}(\underline{x}) + \tilde{u}(\underline{x}, t) + u'(\underline{x}, t)$ , where  $\bar{u}(\underline{x})$  is the ensemble-average,  $\tilde{u}(\underline{x}, t)$  the cyclic component and  $u'(\underline{x}, t)$  the fluctuating component. The phase-averaged velocity is defined as  $\langle u(\underline{x}, t) \rangle = \bar{u}(\underline{x}) + \tilde{u}(\underline{x}, t)$ . The remaining fluctuating component should be seen as a residue characterising events which are

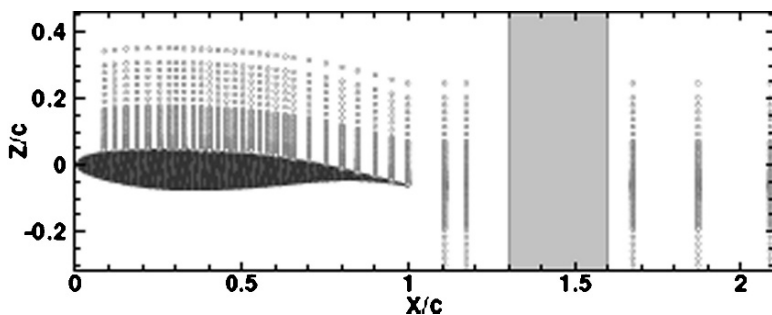


Fig. 1 LDV probing of the flow: definition of the meshing (the shaded region corresponds to a separation between two windows)

not in phase with the reference signal. In the present case, the reference signal has been chosen as the pressure signal measured by the Kulite<sup>TM</sup> transducer located in the mean shock location. The global oscillation of the flow, which can be compared to the global mode provided by the global stability analysis previously described, is characterized by the cyclic component  $\tilde{u}(x, t)$ .

Phase averages of the two-components of the velocity ( $u, v$ ) were determined using the following procedure: (1) the pressure signal measured by the Kulite<sup>TM</sup> transducer located in the mean shock location is used to synchronize the acquisition of LDV signals; (2) the flow period is determined from the low-pass filtered pressure signal and the period is segmented into 20 bins in which data are stored; (3) in each bin, ensemble averages of the velocity (phase averages) and moments of the differences with respect to this phase averages (random fluctuations) are computed.

### 3 Results and Discussion

#### 3.1 Steady Flow Field

We first consider the steady flow field as characterized by the surface pressure distribution. Figure 2 shows a comparison at the sub-critical (steady) condition  $M = 0.73$  and  $\alpha_e = 3.0$  (where the subscript  $e$  signifies the experimental value), with calculations at  $\alpha = 3.0$  and  $\alpha = 3.5$ . The overall agreement is good, but the RANS solution yields a shock position farther downstream than the experiment. However, as the angle of attack is increased the RANS shows a forward movement of the shock – roughly matching the sub-critical experimental location ( $\alpha_e < 3.2$ ) at  $\alpha = 3.5$ . At a fixed Mach number, a higher angle of attack in the RANS results in a slight increase in the roof-top pressure and increased levels of separated flow (with greater unsteadiness, as shown below). This suggests the need for a “Mach correction” in order to match the shock position, the roof-top level and the trailing-edge pressure.

**Fig. 2** Surface pressure coefficient at  $M = 0.73$  from theory ( $\alpha = 3.0^\circ, \alpha = 3.5^\circ$ ) and experiment ( $\alpha_e = 3.0^\circ$ )

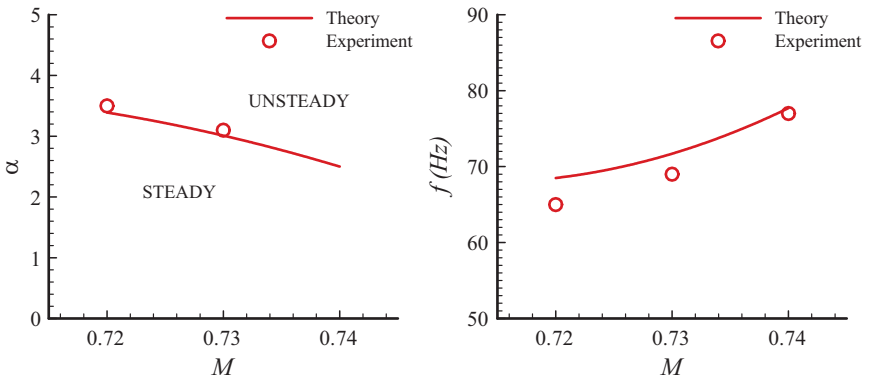
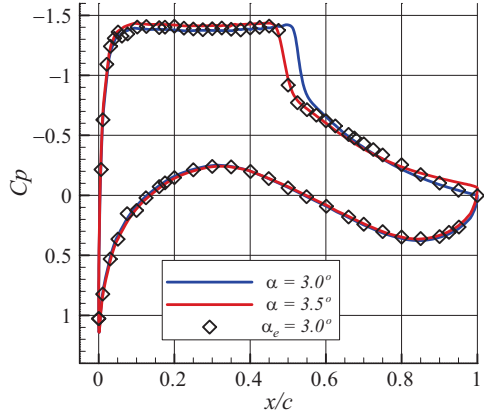


**Fig. 3** Buffet-onset boundary ( $M, \alpha$ ) from theory and experiment, and buffet-onset frequency from theory with frequency at  $\alpha_e = 3.5$  from experiment

These features can be expected to influence the specific point of buffet onset. However, for examining the global flow structure, small differences in the Mach number or angle of attack are not considered significant.

### 3.2 Buffet-Onset Conditions

The global-stability analysis shows the buffet onset results from a Hopf bifurcation. The stability boundary (separating the steady- and unsteady-flow regimes) is shown in Fig. 3, along with the critical-mode frequency. Experimental values for the buffet boundary are given for two of the Mach numbers. The results show that the critical angle of attack for buffet onset decreases with increasing Mach number – consistent

with earlier observations. The frequency at buffet onset increases with increasing Mach number. The experimental frequencies plotted in the figure are for a fixed angle of attack, which is above the critical value. The comparisons show a good agreement between the theory and experiment – especially considering the offset in shock position.

An earlier study using URANS showed that the predicted buffet-onset conditions are influenced by the turbulence model and the treatment of the wind-tunnel walls [5]. Inclusion of the wind-tunnel walls reduced the frequency in the URANS results by 3 Hz. This is comparable to the level of frequency offset seen in Fig. 3.

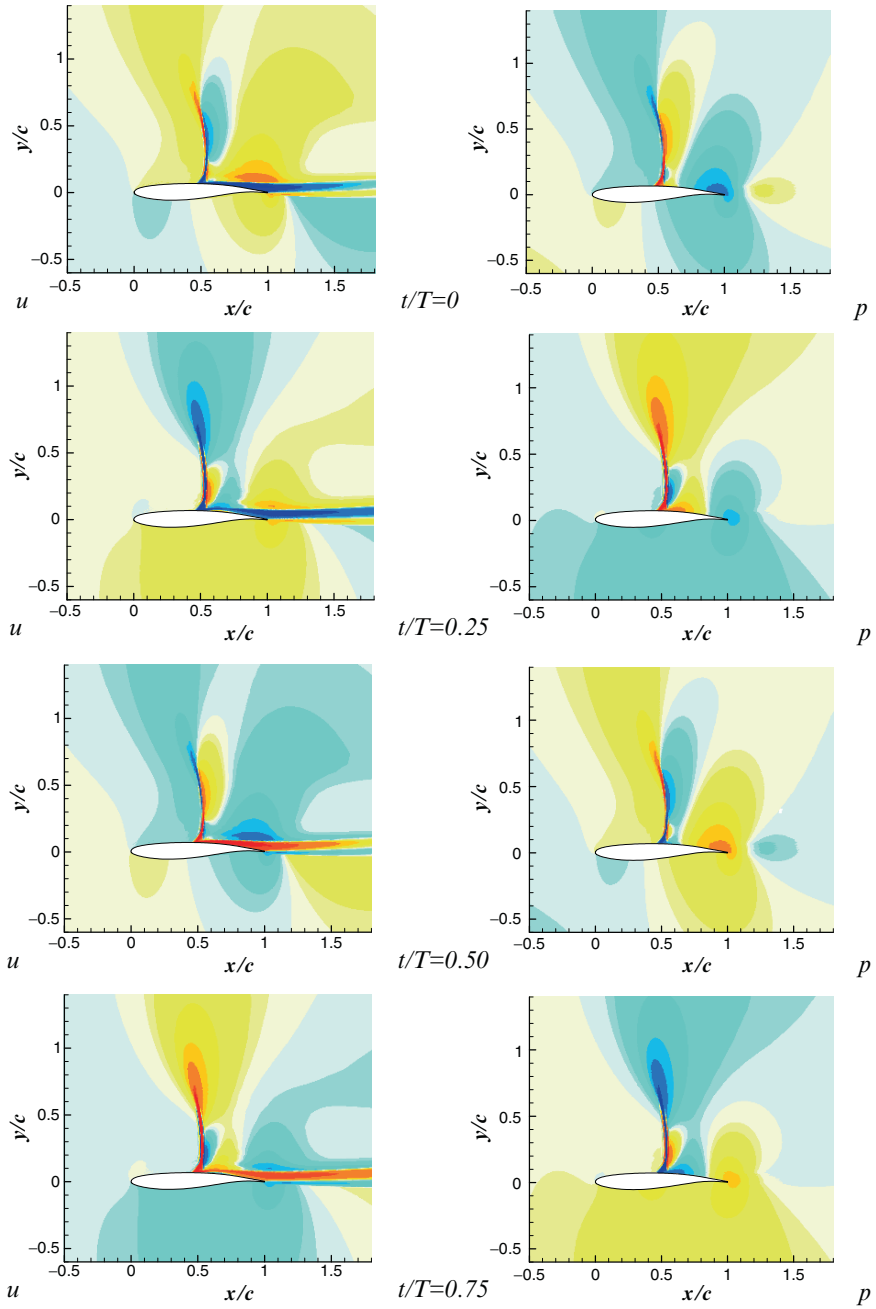
### 3.3 Unsteady Flow Field

The structure of the unsteady flow field is given by the eigenfunction of the global instability. Figure 4 shows the streamwise-velocity and pressure perturbations at four different phases in the oscillation for  $M = 0.73$ ,  $\alpha = 3.5^\circ$  as predicted by the stability theory. The velocity perturbation is concentrated at the shock and in the shear layer downstream of the shock. This velocity perturbation corresponds to an oscillation of the shock coupled with the modulation of the downstream flow – the velocity in the neighbourhood of the shock increases (or decreases) in phase with the velocity variations in the shear layer. Thus, as the shock moves downstream, the shear layer moves toward the airfoil surface. The velocity perturbations extend into the wake, where the downstream evolution shows a periodic increase and decrease in streamwise velocity.

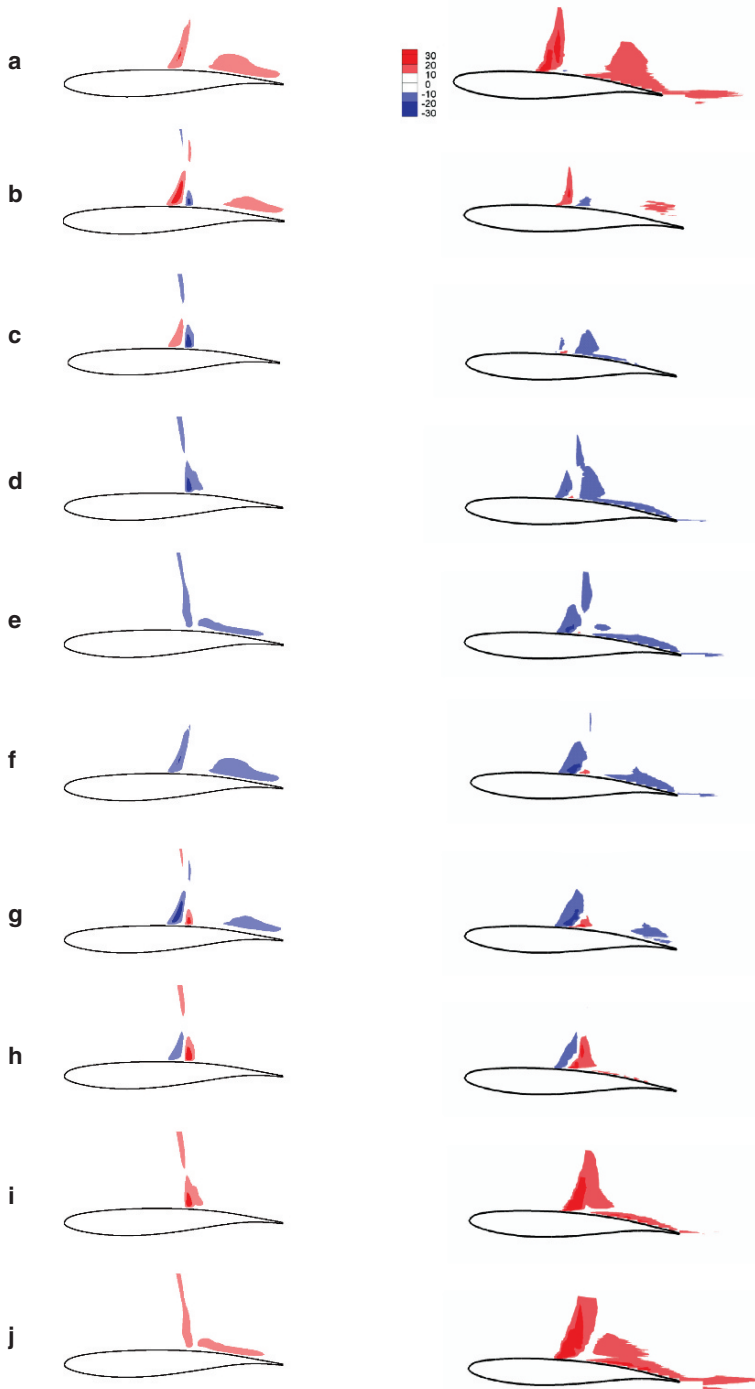
The unsteady pressure is also shown in Fig. 4. The pressure fluctuations appear to originate near the foot of the shock. The disturbance then propagates up away for the surface along the shock. At the same time, the pressure fluctuation (with lower level) propagates downstream in the shear layer. Near the trailing edge the pressure fluctuation intensifies. After rounding the trailing edge, the pressure disturbance propagates upstream along the lower surface.

Figure 5 shows the vertical-velocity fluctuation for conditions similar to Fig. 4. Here the contours are chosen to allow a direct comparison to the flow-field fluctuations measured in the experiments. The figure shows ten phases in the oscillation. The theory and experiment show the same overall structure for the oscillating flow. This supports the global-mode description for the buffeting flow, as given above.

A quantitative look at the unsteady flow is given in Fig. 6, which shows the rms of the surface pressure. The unsteady pressure fluctuations are largest in the neighborhood of the shock, similar to the field perturbation shown in Fig. 4. The pressure fluctuations downstream of the shock are roughly a factor of 5 smaller than the values near the shock. Upstream of the shock, the fluctuations are negligible. The global mode from the stability theory shows the same form for the unsteady surface pressure. In the stability results, the ratio of the pressure fluctuations at, and downstream of, the shock depends on the effective shock thickness.

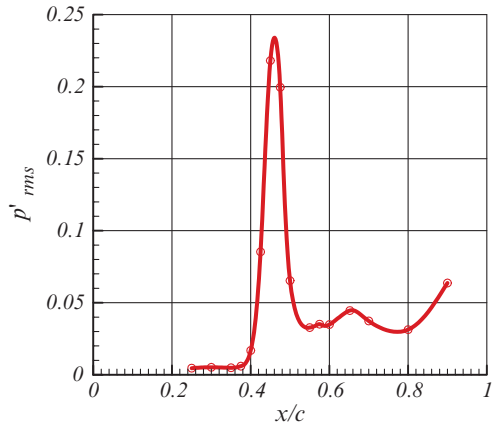


**Fig. 4** Unsteady streamwise  $u$ -velocity (left) and pressure (right) perturbations at  $t/T = 0, 0.25, 0.5, 0.75$  for  $M = 0.73, \alpha = 3.5^\circ$



**Fig. 5** Unsteady  $v$ -velocity fluctuations at  $t/T = 0, 0.1, 0.2 \dots 0.9$  for  $M = 0.73$ ,  $\alpha = 3.5^\circ$ . *Left*: computation (global mode), *right*: experiment (cyclic component of the vertical velocity  $\tilde{v}(\underline{x}, t)$ )

**Fig. 6** Experimental rms of unsteady surface pressure fluctuation for  $\alpha_e = 3.25$ , normalized by the dynamic pressure



## 4 Conclusions

The combination of stability theory and experiment shows the onset of transonic buffeting flow results from global instability. The global mode is characterized by an oscillating shock phased-locked with an oscillating shear layer downstream. The conditions for the onset of buffeting flow, and the buffeting-flow structure, are well predicted by the global-stability theory.

**Acknowledgements** Some of this work was done while the first author was visiting ON-ERA/DAFE in Meudon, France.

## References

1. Crouch, J.D., Garbaruk, A. and Magidov, D., Predicting the onset of flow unsteadiness based on global instability. *J. Comp. Phys.* (2007) doi:10.1016/j.jcp.2006.10.035.
2. McDevitt, J.B. and Okuno, A.F., Static and dynamic pressure measurements on a NACA0012 airfoil in the Ames high Reynolds number facility. NASA Tech. Paper No. 2485 (1985).
3. Jacquin, L., Molton, S., Deck, S., Maury, B. and Soulevant, D., An experimental study of shock oscillation over a transonic supercritical profile. AIAA Paper No. 2005-4902 (2005).
4. Deck, S., Detached-eddy simulation of transonic buffet over a supercritical airfoil. AIAA Paper No. 2004-5378 (2004).
5. Mylène, T. and Coustols, E., Numerical prediction of shock induced oscillations over a 2D airfoil: Influence of turbulence modelling and test section walls. *Int. J. Heat Fluid Flow* **27** (2006) 661–670.
6. Spalart, P.R. and Allmaras, S.R., A one-equation turbulence model for aerodynamic flows. *La Recherche Aéronautique* **1** (1994) 5–21.
7. Spalart, P.R., Trends in turbulence treatments. AIAA Paper No. 2000-2306 (2000).
8. Strelets, M., Detached-eddy simulation of massively separated flows. AIAA Paper No. 2001-0879 (2001).
9. Lehoucq, R.B., Sorensen, D.C. and Yang, C., ARPACK User's Guide, SIAM Publications (1998).

10. Jackson, C.P., A finite-element study of the onset of vortex shedding in flow past variously shaped bodies. *J. Fluid Mech.* **182** (1987) 23–45.
11. Zebib, A., Stability of viscous flow past a circular cylinder. *J. Eng. Math.* **21** (1987) 55–165.
12. Hussain, F. and Reynolds, W., The mechanics of an organized wave in turbulent shear flow. *J. Fluid Mech.* **41** (1970) 241–258.
13. Forestier, N., Jacquin, L. and Geffroy, P., The mixing layer over a deep cavity in a transonic regime. *J. Fluid Mech.*, **475** (2003) 101–145.